European Journal of Radiology Open 13 (2024) 100600

Contents lists available at ScienceDirect

European Journal of Radiology Open

journal homepage: www.elsevier.com/locate/ejro

The value of non-enhanced CT 3D visualization in differentiating stage I invasive lung adenocarcinoma between LPA and non-LPA

Jinxin Chen, Xinyi Zeng, Feng Li, Jidong Peng *

Ganzhou Institute of Medical Imaging, Ganzhou Key Laboratory of Medical Imaging and Artificial Intelligence, Medical Imaging Center, Ganzhou People's Hospital, The Affiliated Ganzhou Hospital of Nanchang University, Ganzhou Hospital-Nanfang Hospital, Southern Medical University, 16th Meiguan Avenue, Ganzhou 341000, PR China

ARTICLE INFO

Keywords:
Lung cancer
Adenocarcinoma
Histological subtype
Three-dimensional visualization
Lepidic predominant adenocarcinoma

ABSTRACT

Objective: This study aims to analyze the quantitative parameters and morphological indices of three-dimensional (3D) visualization to differentiate lepidic predominant adenocarcinoma (LPA) from non-LPA subtypes, which include acinar predominant adenocarcinoma (APA), papillary predominant adenocarcinoma (PPA), micropapillary predominant adenocarcinoma (MPA), and solid predominant adenocarcinoma (SPA).

Methods: A group of 178 individuals diagnosed with lung adenocarcinoma were chosen and categorized into two groups: the LPA group and the non-LPA group, according to their pathological results. Quantitative parameters and morphological indexes such as 3D volume, solid proportion, and vascular cluster sign were obtained using 3D visualization and reconstruction techniques.

Results: Significant differences were observed in the vascular cluster sign, spiculation, shape, air bronchogram, bubble-like lucency, margin, pleural indentation, lobulation, maximum tumor diameter, 3D mean CT value, 3D volume, 3D mass, 3D density, and solid proportion between two groups ($P<0.05$). The optimal cut-off values for diagnosing non-LPA were a 3D mean CT value of −445.45 HU, a 3D density of 0.56 mg·mm^{-3}, and a solid proportion reaching 27.95 %. Multivariate logistic regression analysis revealed that 3D mean CT value, lobulation, and margin characteristics independently predicted stageIinvasive lung adenocarcinoma. The combination of three indicators significantly improved prediction accuracy (AUC=0.881).

Conclusion: The utilization of 3D visualization technology in a systematic approach enables the acquisition of 3D quantitative parameters and morphological indicators of thin-slice CT lesions. These efforts significantly contribute to the identification of histopathological subtypes for stageIinvasive lung adenocarcinoma. When integrated with pertinent clinical data, this offers essential guidance for developing various surgical techniques and treatment plans.

1. Introduction

Lung cancer, a prevalent and deadly form of cancer globally, is responsible for approximately 18 % of all cancer-related deaths [1]. In China, it is notable for having the highest rates of occurrence and fatality among different types of cancer. While the 5-year survival rate for lung cancer can range from 2 % to 30 %, early-stage diagnosis significantly increases the chances of survival to 90 %. This underscores the critical importance of timely and accurate diagnosis for effective treatment [2,3]. The stage and grade of lung cancer pathology play pivotal roles in determining treatment strategies. Patients with stageIor stageIIcancer typically receive recommendations for complete surgical removal, barring any contraindications [4]. Nevertheless, outcomes post-surgery can vary significantly even among patients with the same TNM stage. Distinct morphological characteristics are observed in different lung adenocarcinomas, and even within the same subtype, leading to varying treatment responses according to histological subtypes [5]. As per the 2011 classification of lung adenocarcinoma [6], all pathological specimens were classified based on diverse growth patterns: adherent, acinar, papillary, micropapillary, and solid. These patterns were further categorized into lepidic predominant adenocarcinoma (LPA), acinar predominant adenocarcinoma (APA), papillary predominant adenocarcinoma (PPA), micropapillary predominant adenocarcinoma (MPA), and solid predominant adenocarcinoma (SPA). The prognosis of

* Correspondence to: No.16, MeiGuan Avenue, Ganzhou 341000, PR China.
E-mail address: jidongpeng2021@163.com (J. Peng).

https://doi.org/10.1016/j.ejro.2024.100600
Received 9 July 2024; Received in revised form 4 September 2024; Accepted 10 September 2024

stageIlung adenocarcinoma is significantly influenced by variations in pathological subtypes. The new classification system has shown distinct benefits in predicting recurrence and metastasis [7]. Several studies have consistently shown a lower 5-year survival rate and increased occurrence of lymph node metastasis in cases of MPA [7,8]. Prior to surgery, clinical stageIinvasive lung adenocarcinoma (excluding LPA) frequently exhibits undetected lymph node spread, resulting in a more unfavorable prognosis. Therefore, caution should be exercised when planning sublobar resection for these individuals [9]. Current studies indicate that individuals diagnosed with stageILPA have the potential to reach a disease-free survival rate of 85–90 % over a 5-year period, which represents a notable enhancement compared to non-LPA patients, whose rates vary from 40 % to 65 % [10]. Additionally, the recurrence rate among LPA patients is notably lower than that of non-LPA individuals.

Recent advancements in high-resolution CT, 3D Reconstruction technology, and artificial intelligence (AI) have allowed for the precise construction of 3D morphology of pulmonary nodules. Through the analysis of 3D parameters, researchers have the ability to predict the invasiveness of these nodules [11,12]. Nonetheless, existing studies frequently lack comprehensive indicators for analysis. The optimal diagnostic indicators and their respective cut-off values for forecasting histopathological subtypes of invasive adenocarcinoma are yet to be determined, and the integration of CT three-dimensional parameters in predicting these subtypes has not been implemented in clinical practice. An in-depth assessment of the histopathological subtypes of lung adenocarcinoma before surgery can significantly enhance the tailoring of surgical approaches and therapeutic plans. This investigation seeks to autonomously delineate and obtain 3D quantitative and morphological parameters of lung adenocarcinoma using 3D visualization reconstruction technology. The objective is to pinpoint highly precise diagnostic parameters and their corresponding cut-off values for anticipating histopathological subtypes of lung adenocarcinoma, with a specific emphasis on distinguishing between LPA and non-LPA histopathological subtypes of stage I invasive lung adenocarcinoma.

2. Materials and methods

2.1. Patients

The research protocol underwent scrutiny and gained approval from the Medical Ethics Committee with a waiver of informed consent (approval number: TY-ZKY2024–035–01).

A total of 178 individuals diagnosed with lung cancer received thin-slice CT examinations of the chest followed by radical resection surgery from December 2021 to December 2022. The criteria for inclusion encompassed individuals who had a chest non-enhanced CT scan conducted at our institution within a month prior to the surgery and possessed comprehensive thin-slice CT imaging records. The post-operative pathological findings revealed cases of LPA, APA, PPA, MPA, and SPA, all of which were categorized as stageI. On the other hand, the exclusion criteria involved a medical history of cancerous tumors, simultaneous primary tumors, prior treatment with anticancer medications, past lung surgical procedures, incomplete data from chest CT scans, and uncertain pathological diagnoses. (Fig. 1)

2.2. CT image acquisition

The patient went through a non-enhanced CT scan at the thoracic diaphragm level using a GE Revolution 256-slice CT machine. The scanning parameters used in this study were carefully selected to ensure accurate and detailed imaging. The detector width, measuring 64×0.625 mm, allowed for precise capturing of the scanned data. The field of view (FOV) was set at 40 cm×40 cm, providing a comprehensive view of the scanned area. To achieve optimal image quality, a voltage setting of 120 kV was used. The layer thickness and spacing were both set at 5 mm, ensuring that each individual layer was captured clearly. The pitch ratio of 0.984:1 further enhanced image resolution. Additionally, the current was automatically adjusted to achieve the best results. These scanning parameters were chosen to minimize artifacts and

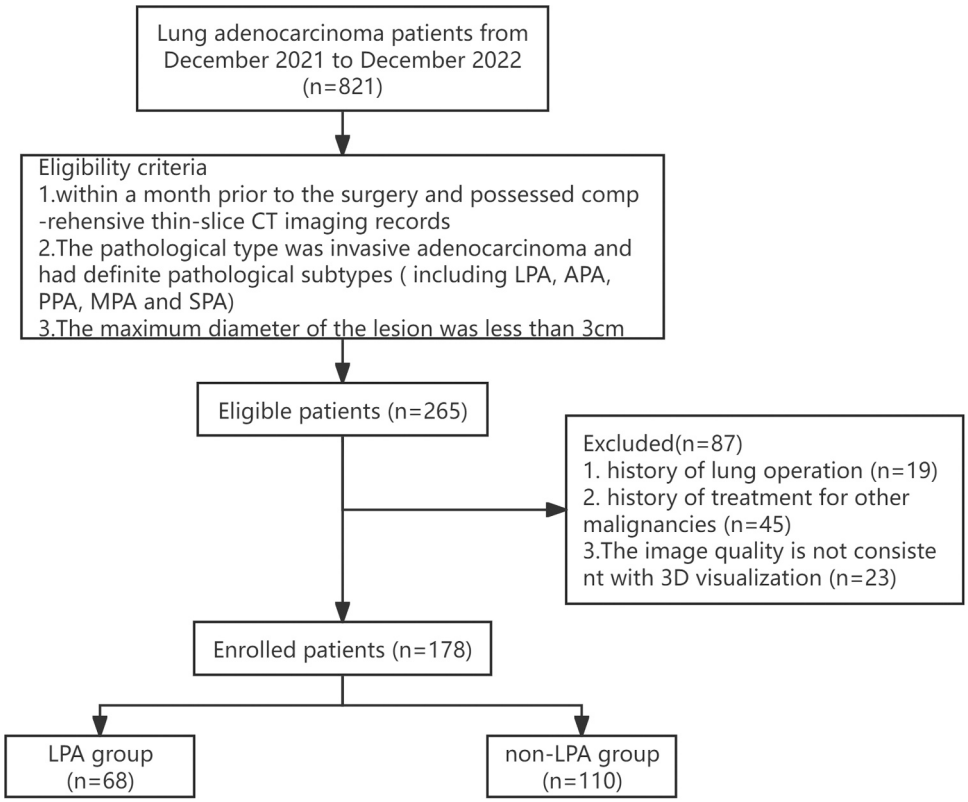

Fig. 1. Overview workflow of this study.

produce high-quality images. Following the initial data gathering, the bone algorithm was employed to conduct post-processing and reassemble the information using a layer thickness and spacing of 1 mm.

CT scan image processing:The DICOM images from PACS were imported into the Synapse 3D software by FUJIFILM Company for image processing. Anonymization of the two-dimensional image data was conducted prior to this step. Following anonymization, the 3D GGN images were reconstructed using semi-automatic mapping. After manually delineating the diameter of the nodule, the entire nodule was automatically extracted and analyzed to obtain the corresponding 3D visualization parameters. (Figs. 2–5)

2.3. CT image evaluation

All CT thin-section images and three-dimensional visualization reconstructed images were independently delineated and observed by two physicians. Physician 1 had 2 years of experience in radiological diagnosis, while Physician 2 had 10 years of experience. Continuous variables were evaluated using the intraclass correlation coefficient (ICC), while the consistency within and between observers for ordered and unordered categorical variables was assessed using the weighted Kappa coefficient and Cohen's Kappa coefficient, respectively. An ICC value greater than 0.75 indicates good consistency, while a Kappa value between 0.8 and 1.0 indicates a strong degree of consistency. The results of Physician 1's initial delineation and observation were ultimately considered. All study participants were kept uninformed about the patient's diagnosis, following the double-blind principle. The CT image review involved using a lung window (width: 1600 HU, horizontal: −600 HU) and a mediastinal window (width: 400 HU, horizontal: 40 HU). The following parameters were collected and recorded for GGN: Maximum tumor diamete, 3D mean CT value, 3D volume, solid proportion, vascular cluster sign, air bronchogram, access of vascular into lesion, bubble-like lucency, pleural indentation, spiculation, lobulation, shape, and margin. Based on these parameters, 3D density and 3D mass were calculated as follows [13]: 3D physical density$\rho(mg/mm^3)$ = (3D mean CT value + 1000) / 1000, 3D mass (mg) = (3D mean CT value + 1000) / 1000 × 3D volume (mm^3).

2.4. Statistical analysis

Analysis of data and creation of graphics were carried out using IBM SPSS 26.0 and GraphPad 8.3 software. Intraclass correlation coefficients were computed to evaluate agreement among continuous variables. The weighted Kappa coefficient was applied to assess inter-observer agreement for ordered categorical variables, whereas Cohen's Kappa coefficient was employed for unordered categorical variables. A T test was conducted on independent samples to analyze normally distributed measurement data, with results presented as Mean±SD. For non-normally distributed measurement data, outcomes were expressed as Median (1st quartile, 3rd quartile) and analyzed using the Mann-Whitney U test. Percentages were utilized to report numerical data, and comparison between groups was done using either the Chi-square or Fisher exact probability test. Receiver Operating Characteristic curves (ROC) were used to investigate significant variations in quantitative parameters, with determination of optimal diagnostic thresholds for each parameter through the calculation of the Youden index (YI) and evaluation of the Area Under the Curve (AUC), sensitivity, and specificity. Logistic regression analysis was carried out to identify independent risk factors affecting the histopathological type of lung adenocarcinoma, leading to the construction of a multivariate regression diagnostic model (Log P model). The significance level was set at 0.05, unless otherwise specified.

Fig. 2. Non-enhanced two-dimensional CT images of a lesion.

Fig. 3. Semi-automatic Region of Interest (ROI) Delineation and automatic analysis.

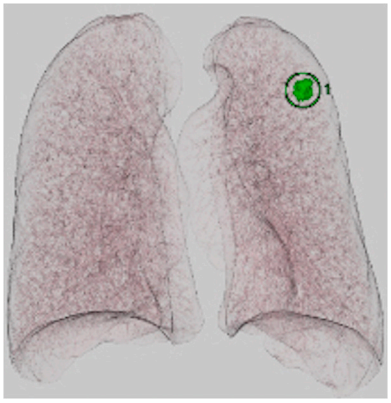

Fig. 4. Example of 3D visualization results of a lesion.

Fig. 5. Example of 3D visualization results of a lesion.

3. Result

3.1. Interobserver agreement assessment

The Radiologists demonstrated good diagnostic consistency across a range of factors for all patients, including Maximum tumor diameter, 3D mean CT value, 3D volume, solid proportion, vascular cluster sign, air bronchogram, access of vascular into lesion, bubble-like lucency, pleural

indentation, spiculation, lobulation, shape, and margin. The ICC values or Kappa values calculated for these factors were statistically significant at P<0.05, with values of 0.998, 0.960, 1.000, 0.993, 0.920, 0.872, 0.857, 0.893, 0.951, 0.852, 0.891, 0.901, and 0.812.

3.2. General data comparison

The study included 178 individuals who had been identified with stageIlung adenocarcinoma. Out of these, 68 individuals were part of the LPA category, with an average age of 57 (49,67), while the non-LPA group consisted of 110 patients with an average age of 59 (52,63). A comparison was conducted between the LPA group (LPA) and the non-LPA group (APA/PPA/MPA/SPA). Maximum tumor diameter were divided into categories of less than 1 cm (17 vs 14 cases), 1–2 cm (45 vs 69 cases), and more than 2 cm (6 vs 27 cases), displaying statistically significant variances (P<0.05). (Table 1)

3.3. Thin-slice CT finding

Significant statistical variances were noted in the vascular cluster sign, spiculation, shape, air bronchogram, bubble-like lucency, pleural indentation, lobulation and margin among the two groups of lung adenocarcinoma (P<0.05). (Table 2)

3.4. Three dimensional quantitative parameter in LPA vs non-LPA

The non-LPA group exhibited significantly higher values in Maximum tumor diameter, 3D mean CT value, 3D volume, 3D density, 3D mass, and solid proportion compared to the LPA group (P < 0.05). These findings indicate that these indicators could potentially aid in distinguishing between histopathological subtypes of invasive adenocarcinoma, such as LPA and non-LPA. (Table 3 and Figs. 6–11)

3.5. Efficacy of univariate analysis in predicting LPA versus non-LPA

The optimal threshold cut-off point for predicting pathological subtypes in the two groups based on the 3D mean CT value was determined to be −445.45 HU, yielding an AUC of 0.764. The sensitivity and specificity were measured at 56.4 % and 85.3 % respectively. Similarly, the optimal thresholds for 3D density and 3D quality were identified as 0.56 mg·mm^{-3} and 388.23 mg, with AUCs of 0.764 and 0.707. Sensitivity for 3D density was 56.4 % with specificity at 73.6 %, while for 3D quality it was 56.4 % and 63.2 %. Moreover, the optimal threshold for solid component in forecasting pathological subcategories was established at 27.95 %, showcasing an AUC of 0.776 with sensitivity and specificity rates of 60.0 % and 88.2 % correspondingly. (Table 4 and Fig. 12).

Table 1
Comparison of general data between two groups of stage I invasive lung adenocarcinoma.

Characteristics	LPA(n=68)	non-LPA(n=110)	P value
Age(years)	57(49,67)	59(52,63)	0.719
Age distribution			0.872
<40 years old	7(10.3)	9(8.2)	
40–60 years old	34(50.0)	58(52.7)	
>60 years old	27(39.7)	43(39.1)	
Gender			0.568
Male	27(39.7)	39(35.5)	
Female	41(60.3)	71(64.5)	
Maximum tumor diameter			0.009
<1 cm	17(25.0)	14(12.7)	
1–2 cm	45(66.2)	69(62.7)	
>2 cm	6(8.8)	27(24.6)	
Location			0.118
Right upper lobe	33	37	
Right middle lobe	5	5	
Right lower lobe	13	29	
Left upper lobe	12	22	
Left lower lobe	5	17	

Note:The results are reported as Median (first quartile, third quartile) or No. (%). LPA: lepidic predominant adenocarcinoma, non-LPA (including acinar predominant adenocarcinoma (APA), papillary predominant adenocarcinoma (PPA), micropapillary predominant adenocarcinoma (MPA), and solid predominant adenocarcinoma (SPA)).

Table 2
Morphological comparison of invasive lung adenocarcinoma between two groups.

Thin-section features	LPA(n=68)	non-LPA(n=110)	P value
Shape			
Round	53(77.9)	53(48.2)	<0.001
irregular	15(22.1)	57(51.8)	
Margin			<0.001
Clear	19(27.9)	3(2.7)	
Obscure	49(72.1)	107(97.3)	
Air bronchogram			0.009
Present	6(8.8)	27(24.5)	
Absent	62(91.2)	83(75.5)	
Bubble-like lucency			0.011
Present	11(16.2)	37(33.6)	
Absent	57(83.8)	73(66.4)	
Pleural indentation			<0.001
Present	6(8.8)	42(38.2)	
Absent	62(91.2)	68(61.8)	
Access of vascular into lesion			0.615
Present	19(27.9)	27(24.5)	
Absent	43(61.4)	83(75.5)	
Spiculation			<0.001
Present	10(14.7)	75(68.2)	
Absent	58(85.3)	35(31.8)	
Lobulation			<0.001
Present	11(16.2)	87(79.1)	
Absent	57(83.8)	23(20.9)	
Vascular cluster sign			<0.001
Present	23(33.8)	90(81.8)	
Absent	45(66.2)	20(18.2)	

Note: Data are presented as No. (%). See Table 1 legend for expansion of other abbreviations.

Table 3
Comparison of quantitative parameters between two groups of stage I invasive lung adenocarcinoma.

3D CT Image Parameters	LPA(n=68)	non-LPA(n=110)	P value
Maximum tumor diameter (mm)	12.55(9.93,17.08)	15.00(12.00,20.08)	0.003
3D mean CT value (HU)	−595.15 (−657.93,−496.50)	−412.30 (−551.45,−139.70)	<0.001
3D volume (mm^3)	757.00 (465.68,1442.30)	1297.45 (734.80,2196.25)	0.002
3D density (mg*mm^{-3})	0.40(0.34,0.50)	0.58(0.44,0.86)	<0.001
3D mass (mg)	303.44 (195.70,925.94)	760.87 (326.91,1511.33)	<0.001
solid proportion (%)	13.90(5.53,22.98)	37.95(16.08,80.45)	<0.001

Note: Data are presented as Median (first quartile, third quartile). HU: Hounsfield units. 3D: three dimensional. See Table 1 legend for expansion of other abbreviations.

3.6. Prediction of LPA and non-LPA performance by multivariate analysis

The study performed a univariate analysis to detect variables that showed statistical significance. These variables were then utilized in binary logistic regression using the stepwise method to determine the factors that influenced LPA in stage I invasive lung adenocarcinoma. The findings revealed that 3D mean CT value, lobulation, and margin served

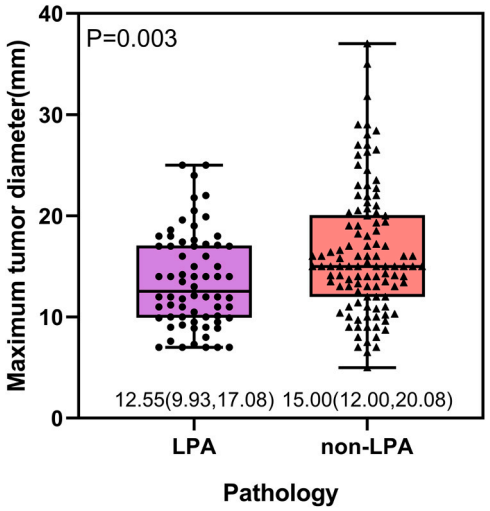

Fig. 6. Maximum tumor diameter in lepidic predominant adenocarcinoma (LPA) vs non-LPA (including acinar predominant adenocarcinoma (APA), papillary predominant adenocarcinoma (PPA), micropapillary predominant adenocarcinoma (MPA), and solid predominant adenocarcinoma (SPA)).

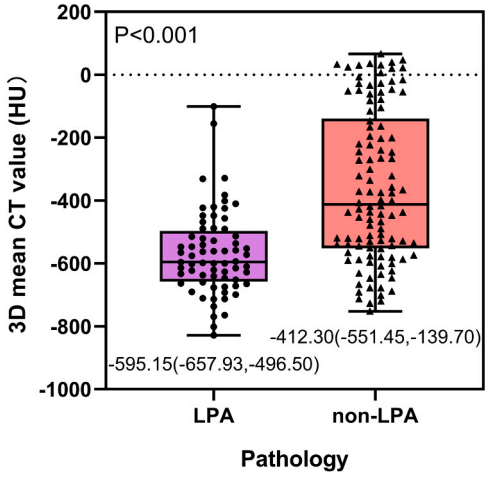

Fig. 7. 3D mean CT value in LPA vs non-LPA.

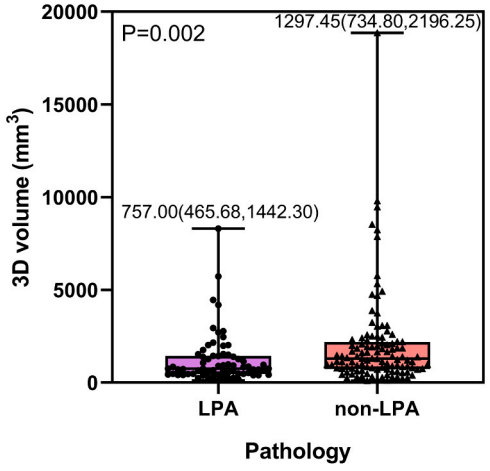

Fig. 8. 3D volume in LPA vs non-LPA.

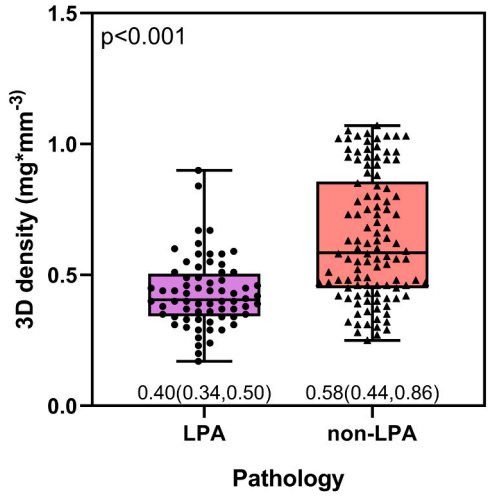

Fig. 9. 3D density in LPA vs non-LPA.

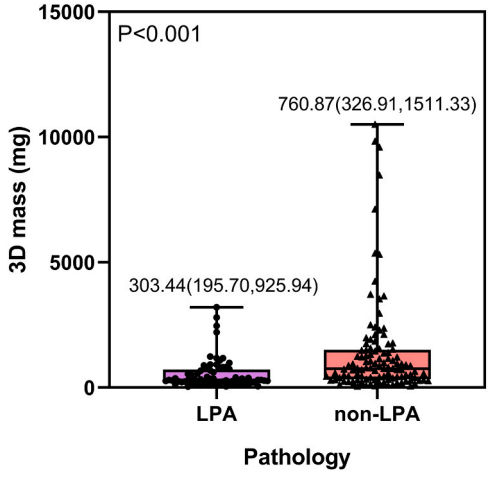

Fig. 10. 3D mass in LPA vs non-LPA.

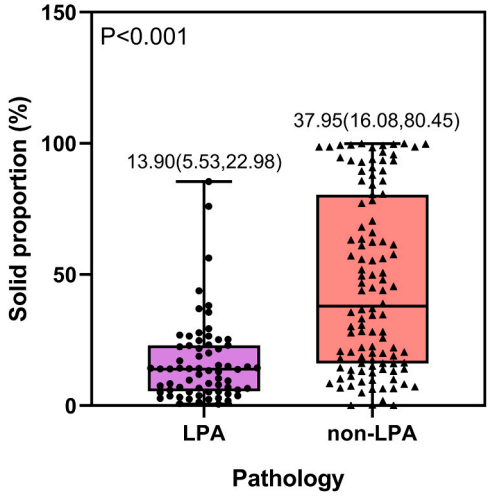

Fig. 11. Solid proportion in LPA vs non-LPA.

as independent predictors of LPA in individuals with stage I invasive lung adenocarcinoma. The analysis resulted in a regression formula of logit (P) = 1.624 + 0.004×3D mean CT value + 2.156× lobulation +

Table 4
Univariate analysis of lung adenocarcinoma related quantitative parameters.

3D CT Image Parameters	AUC	95 %CI	P value	Threshold	Sensitivity%	Specificity%	Youden index
Maximum tumor diameter (mm)	0.628	(0.544,0.711)	0.004	12.30	74.5	50.0	0.245
3D mean CT value (HU)	0.764	(0.695,0.833)	<0.001	−445.45	56.4	85.3	0.417
3D volume (mm^3)	0.638	(0.554,0.721)	0.002	765.25	73.6	52.9	0.265
3D density ($mg*mm^{-3}$)	0.764	(0.695,0.833)	<0.001	0.56	56.4	85.3	0.417
3D mass (mg)	0.707	(0.629,0.784)	<0.001	388.23	73.6	63.2	0.368
solid proportion (%)	0.776	(0.709,0.843)	<0.001	27.95	60.0	88.2	0.482

Note: AUC:the area under the curve. CI: confidence interval. See Table 3 legend for expansion of other abbreviations.

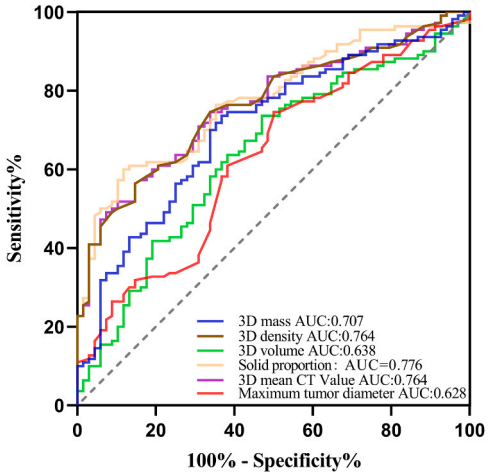

Fig. 12. ROC curve of Maximum tumor diameter, 3D mean CT value, 3D volume, 3D density, 3D mass, and solid proportion for predicting LPA and non-LPA.

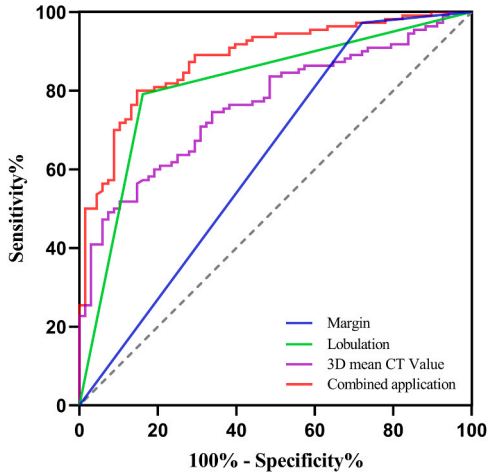

Fig. 13. 3D mean CT value, lobulation sign, margin, and combined ROC curves.

1.736× margin. The investigation determined that the likelihood of a rough boundary in LPA was lower compared to non-LPA (OR = 0.176, 95 %CI: 0.046–0.682). Furthermore, the 3D mean CT value was lower in the LPA group than in the non-LPA group (OR = 1.004, 95 %CI: 1.001–1.007). Lastly, the probability of the lobulation sign in LPA was lower than in non-LPA (OR = 8.637, 95 %CI: 3.633–20.530).(Table 5)

The table above illustrates that the 3D mean CT value, lobulation, and margin can each independently predict LPA in stage I invasive lung adenocarcinoma with statistical significance ($P < 0.05$). Using a combination of these three indicators enhances the diagnostic efficacy for predicting LPA. Analysis of the ROC curve utilizing this particular combination yielded an AUC of 0.881, showing a sensitivity of 80.0 % and a specificity of 85.3 %, with a confidence interval of 95 % ranging from 0.832 to 0.931. (Fig. 13)

4. Discussion

Non-small cell lung cancer, also referred to as NSCLC, makes up around 80 % of lung cancer cases, with adenocarcinomas accounting for roughly 60 % [14]. Timely detection and swift medical intervention play a crucial role in improving patient prognoses. Research has indicated a connection between histological subtypes of early lung adenocarcinoma and prognosis, where LPA is associated with a more positive outlook compared to non-LPA subtypes (APA, PPA, MPA, SPA) [15]. The objective of this research is to utilize cutting-edge three-dimensional visualization technology for the semi-automated delineation of lesions, generating a 3D representation that captures both quantitative CT metrics and morphological characteristics of the lesion. Through the analysis of the lesion from various viewpoints, particularly emphasizing pleural and bronchial vessel structure, the study seeks to pinpoint the most accurate reference parameter for forecasting histopathological subcategories. This data can be valuable in guiding the selection of optimal surgical methods and therapeutic plans in practical medical scenarios.

This research emphasizes the significance of employing quantitative parameters in three dimensions for a thorough examination of lesions. By taking into account factors like volume, intensity, and mass from different viewpoints, a broader range of statistically notable information can be gathered. In contrast to conventional techniques that depend on 2D sketches, the application of 3D imaging technology enables a more precise depiction of the complete lesion. Scholars including Kitazawa and colleagues [16] have underscored the importance of features like the average CT value in lesion assessment in three dimensions, surpassing the constraints of 2D CT assessments. Similarly, research conducted by Guangyao et al. [17] has highlighted the advantages of categorizing lesions into solid and ground glass components, quantifying their 3D volumes and CT values, and constructing models for lesion assessment, which surpassed alternative diagnostic methods. An association between the size and CT attenuation of the lesion and the degree of invasiveness of the lesion was observed. Kitami et al. [18] investigated pure ground glass nodules and determined an average CT value of 600 HU as the ideal threshold for distinguishing non-invasive and invasive lesions. Limited imaging investigations have been carried out

Table 5
Multivariate Logistic regression of histopathological subtypes of lung adenocarcinoma.

Variables	β-value	SE value	Wald value	P value	OR value	95 %CI
constant	1.624	0.831	3.823	0.051	5.075	
3D mean CT value (HU)	0.004	0.001	8.021	0.005	1.004	1.001,1.007
Lobulation	2.156	0.442	23.819	<0.001	8.637	3.633,20.530
Margin	1.736	0.691	6.320	0.12	0.176	0.046,0.682

Note: CI: confidence interval. 3D: three dimensional.

on the histopathological subtypes of stageIlung adenocarcinoma. Zhang et al. [19] revealed that the mean CT value of the LPA category was lower than that of the non-LPA category ($P < 0.05$). Distinguishing early lung adenocarcinoma with partial solid nodules through improved 3D CT reconstructions, the classification of adenocarcinoma in situ, minimally invasive adenocarcinoma, and LPA was labeled as low-risk by You et al. [20], while APA, PPA, and MPA were categorized as high-risk. The investigation demonstrated that the average 3D CT value was the most reliable predictor between the two categories. The findings suggested that a 3D mean CT value of −445.45 HU represented the optimal threshold for distinguishing LPA from non-LPA, and a multivariate logistic regression analysis affirmed that the 3D mean CT value was an autonomous predictor. The relatively diminished density of non-LPA lesions may be attributed to factors such as alveolar wall expansion, normal air composition in the alveoli, lack of alveolar collapse, blood vessel, and bronchus intrusion [21].

The research findings indicated notable variations in 3D volume, 3D mass, and 3D density among the LPA and non-LPA cohorts. Of particular interest was the statistical divergence in 3D density, where a threshold of 0.56 $mg{\cdot}mm^{-3}$ resulted in an area under the ROC curve of 0.766, signifying moderate diagnostic effectiveness. Increased likelihood of malignancy was associated with the presence of a solid component, particularly larger solid components within nodules, which showed a direct relationship with the risk of malignancy. A prior investigation by Nakata et al. [22] provided evidence that ground-glass nodules containing extended solid components were more likely to be cancerous growths. Notably, tumor size emerged as a critical prognostic indicator, with LPA nodules generally presenting with smaller diameters in comparison to SPA, APA, and MPA nodules. This observation was corroborated by Shi et al. [23], who noted higher malignancy rates in pulmonary nodules exceeding 10 mm in size. Furthermore, the analysis unveiled a significant difference in the maximal diameter of lesions between the LPA and non-LPA populations, highlighting the limited diagnostic utility of employing this criterion as the sole determinant for LPA classification.

The morphological characteristics revealed through 3D visualization offer a more in-depth understanding of lesions. In this research, it was found that non-LPA lesions were significantly more likely to display lobulation in comparison to LPA lesions (79.1 % vs 16.2 %). The existence of lobulation is associated with the size of the tumor [24]. Smaller tumors tend to exhibit round or round-like lobulation, with tumors measuring 1–1.5 cm leading to lobulation. As tumors increase in size, lobulation becomes more prominent, and irregular growth patterns can emerge. Pathologically, lobulation is associated with different degrees of cellular differentiation, inhibition of tumor growth due to surrounding lung tissue, and the tightening of fibrous tissue within the lesion, leading to varying growth rates [25]. The identification of the vascular convergence sign is a key marker for malignant tumors, as angiogenesis plays a crucial role in tumor progression and spread [26]. Overproduction of vascular endothelial growth factor and the proliferation of vascular endothelial cells during angiogenesis lead to the formation of immature tumor blood vessels that are highly porous, resulting in edema within the tumor tissue. The research indicated a higher frequency of vascular convergence in the non-LPA group (81.8 % or 90 out of 110 cases), although it was also detected in 33.8 % (23 out of 68 cases) of the LPA group. The presence of the bubble-like sign, characterized by circular or branched air attenuation within the lesion, signifies squamous growth of adenocarcinomas along lung structures and bronchi. The air bronchogram may show slight distortion or dilation [27], particularly in cases where a fibro-connective tissue proliferative reaction occurs within the tumor. This research found that the vacuole sign was more common in the non-LPA group than in the LPA group. Lung adenocarcinomas with solid components tend to exhibit the pleural indentation sign. Central fibrosis and tissue contraction can cause peripheral fiber bundles to form around the tumor, resulting in a linear shadow between the tumor and the pleura. This shadow signifies pleural indentation on CT scans [28]. As the lesion becomes more invasive, the level of fibrosis typically increases, resulting in a significant increase in pleural indentation with higher histological grades [29]. The demarcation line between the tumor and adjacent healthy lung tissue is typically visibly irregular in the majority of malignant pulmonary nodules because of the invasive nature of the tumor's growth pattern [30]. Our results indicate that a well-defined or rough interface can effectively differentiate between LPA and non-LPA. Spiculation is caused by direct tumor invasion of nearby bronchial vascular sheaths, local lymph node expansion, or radiation of fibrous lines into the peripheral lung fields due to the desmoplastic reaction of the nodules [31]. Kuriyama and colleagues [32] reported that air bronchograms were present in the majority of malignant tumors, possibly due to tumor cell invasion into the bronchus or bronchiole, resulting in changes in the cartilage or elastic layer and subsequent airway distortion and dilation. This study found a higher likelihood of observing an air bronchial sign in the non-LPA group (24.5 %) compared to the LPA group (8.8 %).

The results of this research show that 3D mean CT value, lobulation, and margin can function as separate indicators for differentiation of LPA and non-LPA in early-stage invasive lung adenocarcinoma. Integration of 3D mean CT value, lobulation, and margin can greatly improve the precision of diagnosis for LPA. It is important to mention that the absence of statistical significance in the sign of main vessel passage between LPA and non-LPA groups could be due to the utilization of unenhanced scan images rather than enhanced scans in this study.

This research has some limitations. To start with, the data is sourced from just one center, meaning the results may not be representative of other centers. To support and strengthen our results, it is recommended that future research be conducted at multiple research centers. Additionally, it is important to note that our study was limited to a specific group of lesions larger than 2 cm in size, which may have influenced the outcome of the data analysis.

5. Conclusion

Radiologists can significantly aid in distinguishing between histopathological subtypes of stage I invasive lung adenocarcinoma by strategically utilizing three-dimensional visualization technology to analyze quantitative parameters and morphological indicators of thin-slice CT lesions. When combined with pertinent clinical data, this methodology has important implications for guiding the selection of suitable surgical techniques and treatment plans in a clinical environment.

Ethics

The research protocol underwent scrutiny and gained approval from the Medical Ethics Committee with a waiver of informed consent (approval number: TY-ZKY2024–035–01).

Funding

This work received funding from two sources: the special fund for Postgraduate Innovation In Jiangxi Province, China (YC2023-S192) and the Clinical Research Center for Medical Imaging in Jiangxi Province, China (20223BCG7400199).

CRediT authorship contribution statement

Jinxin Chen: Writing – review & editing, Writing – original draft, Visualization, Validation, Supervision, Software, Resources, Project administration, Methodology, Investigation, Funding acquisition, Formal analysis, Data curation, Conceptualization. **Xinyi Zeng:** Validation, Software, Project administration, Methodology, Investigation, Formal analysis, Data curation. **Feng Li:** Visualization, Software, Resources, Investigation, Formal analysis, Data curation. **Jidong Peng:** Writing – review & editing, Writing – original draft, Visualization,

Supervision, Resources, Project administration, Methodology, Investigation, Funding acquisition, Formal analysis, Data curation, Conceptualization.

Declaration of Competing Interest

No conflict of interest exits in the submission of this manuscript, and manuscript is approved by all authors for publication. I would like to declare on behalf of my co-authors that the work described was original research that has not been published previously, and not under consideration for publication elsewhere, in whole or in part. All the authors listed have approved the manuscript that is enclosed.

Acknowledgments

This work received funding from two sources: the special fund for postgraduate innovation in Jiangxi province, China (YC2023-S192) and the clinical research center for medical imaging in Jiangxi province, China (20223BCG7400199).

References

[1] H. Sung, et al., Global Cancer Statistics 2020: GLOBOCAN Estimates of Incidence and Mortality Worldwide for 36 Cancers in 185 Countries, CA Cancer 71 (2021) 209–249.
[2] W. Cao, H.D. Chen, Y.W. Yu, et al., Changing profiles of cancer burden worldwide and in China: a secondary analysis of the global cancer statistics 2020, Chin. Med. 134 (2021) 783–791.
[3] M.B. Schabath, M.L. Cote, Cancer progress and priorities: lung cancer, Cancer Epidemiol. Biomark. Prev. 28 (10) (2019) 1563–1579.
[4] N. Duma, R. Santana-Davila, J.R. Molina, Non-small cell lung cancer: epidemiology, screening, diagnosis, and treatment, Mayo Clin. Proc. 94 (2019) 1623–1640.
[5] J.A. Barletta, B.Y. Yeap, L.R. Chirieac, Prognostic significance of grading in lung adenocarcinoma, Cancer 116 (2010) 659–669.
[6] W.D. Tmvis, E. Brambills, M. Noguchi, et al., International association for the study of lung cancer/American thoracic society/European respiratory society international muhidisciplinary classification of lung adenocarcinoma, Thorac. Oncol. 6 (2011) 244–285.
[7] A. Yoshizawa, N. Motoi, G.J. Riely, et al., Impact of proposed IASLC/ATS/ERS classification of lung adenocarcinoma: prognostic subgroups and implications for further revision of staging based on analysis of 514 stageIcases, Mod. Pathol. 24 (2011) 653–664.
[8] A. Warth, T. Muley, M. Meister, et al., The novel histologic International Association for the Study of Lung Cancer/American Thoracic Society/European Respiratory Society classification system of lung adenocarcinoma is a stage-independent predictor of survival, Clin. Oncol. 30 (2012) 1438–1446.
[9] H. Ito, H. Nakayama, S. Murakami, et al., Does the histologic predominance of pathological stage IA lung adenocarcinoma influence the extent of resection, Gen. Thorac. Cardiovasc Surg. 65 (2017) 512–518.
[10] J. Chen, M. Yuan, Y. Zhong, et al., Differential value of CT quantitative analysis for different subtypes of invasive lung adenocarcinoma presenting as subsolid nodule, J. Pract. Radiol. 35 (2019) 887–891.
[11] M. Shi, L.Y. Xu, X.F. Pan, et al., Diagnostic value of there-dimensional reconstruction technique in new classification criteria of lung adenocarcinoma, Chin. J. Clin. Thorac. Cardiovasc. Surg. 28 (3) (2021) 278–282.
[12] G. Chassagnon, M. Vakalopoulou, N. Paragios, et al., Artificialintelligence applications for thoracic imaging, Eur. J. Radio. 123 (2020) 108774.
[13] E.T. Cao, H. Yu, L. Fan, et al., Quantitative CT analysis of early-stage lung adenocarcinoma with pure ground-glass opacity, Chin. J. Radiol. 50 (12) (2016) 940–945.
[14] A. Jemal, R. Siegel, J. Xu, et al., Cancer statistics, 2010 CA Cancer J. Clin. 60 (2010) 277–300.
[15] Y.C. Hou, W.J. Song, M.Z. Chen, et al., The presence of lepidic and micropapillary/solid pathological patterns as minor components has prognostic value in patients with intermediate-grade invasive lung adenocarcinoma, Transl. Lung Cancer Res 11 (1) (2022) 64–74.
[16] Guangyao Wu, Henry C. Woodruff, Jing Shen, et al., Diagnosis of invasive lung adenocarcinoma based on chest CT radiomic features of part-solid pulmonary nodules: a multicenter study. Radiology Vol.297 (2) (2020) 0.
[17] L.L. Qi, B.T. Wu, W. Tang, et al., Long-term follow-up of persistent pulmonary pure ground-glass nodules with deep learning-assisted nodule segmentation, Eur. Radio. 30 (2) (2020) 744–755.
[18] A. Kitami, F. Sano, S. Hayashi, et al., Correlation between histological invasiveness and the computed tomography value in pure groundglass nodules, Surg. Today 46 (2016) 593–598.
[19] P. Zhang, T. Li, X. Tao, et al., HRCT features between lepidic-predominant type and other pathological subtypes in early-stage invasive pulmonary adenocarcinoma appearing as a ground-glass nodule, BMC Cancer 21 (2021) 1124.
[20] J. You, G. Zhang, X. Gao, et al., Value of PET /CT Combined with CT Three-dimensional Reconstruction in distinguishing different pathological subtypes of early lung adenocarcinoma, Zhongguo Fei Ai Za Zhi 24 (2021) 468–474.
[21] W. Xiang, Y. Xing, S. Jiang, et al., Morphological factors differentiating between early lung adenocarcinomas appearing as pure ground-glass nodules measuring ≤10 mm on thin-section computed tomography, Cancer Imaging 14 (2014) 33.
[22] M. Nakata, H. Saeki, I. Takata, et al., Focal ground-glass opacity detected by low-dose helical CT, Chest 121 (2002) 1464–1467.
[23] C.Z. Shi, Q. Zhao, L.P. Luo, J.X. He, Size of solitary pulmonary nodule was the risk factor of malignancy, Thorac. Dis. 6 (2014) 668–676.
[24] M.M. Wahidi, J.A. Govert, R.K. Goudar, et al., Evidence for the treatment of patients with pulmonary nodules: when is it lung cancer?: ACCP evidence-based clinical practice guidelines (2nd edition), Chest 132 (3 Suppl) (2007) 94s–107s.
[25] H. Cheng, X.M. Zhang, S.Z. Liang, et al., Correlation between pathological differentiation and CT ground-glass nodule in peripheral lung adenocarcinomas, Pr. Radio. 39 (10) (2023) 1593–1596.
[26] H. Wang, Y.Y. Yan, F.Z. Gong, et al., nalysis of risk factors for the expression of TRIM28 and LAPTM4B in lung adenocarcinoma based on high-resolution CT image features and texture parameters, Radiol. Pract. 36 (9) (2021) 1101–1105.
[27] A. Birau, R.A. Ceausu, A.M. Cimpean, et al., Assessement of angiogenesis reveals blood vessel heterogeneity in lung carcinoma, Oncol. Lett. 4 (2012) 1183–1186.
[28] X.H. Pu, M. Yan, T.Y. Chen, et al., Preoperative evaluation of visceral pleural invasion of lung adenocarcinoma with MSCT, Pr. Radio. 35 (4) (2019) 549–553.
[29] K. Kuriyama, R. Tateishi, O. Doi, et al., CT-pathologic correlation in small peripheral lung cancers, AJR Am. J. Roentgenol. 149 (1987) 1139–1143.
[30] H.Y. Kim, Y.M. Shim, K.S. Lee, et al., Persistent pulmonary nodular ground-glass opacity at thin-section CT: histopathologic comparisons, Radiology 245 (2007) 267–275.
[31] J. Liang, X.Q. Xu, H. Xu, et al., Using the CT features to differentiate invasive pulmonary adenocarcinoma from pre-invasive lesion appearing as pure or mixed ground-glass nodules, Br. J. Radiol. 88 (2015) 20140811.
[32] K. Kuriyama, R. Tateishi, O. Doi, et al., Prevalence of air bronchograms in small peripheral carcinomas of the lung on thin-section CT: comparison with benign tumors, AJR 156 (1991) 921–924.